Preprint Title	Quantum Chemical Investigation of the Formation of Spiroheterocyclic Compounds Via the (3 + 2) Cycloaddition Reaction of 1-methyl-3-(2,2,2-trifluoroethylidene)pyrrolidin-2-one with Diazomethane and Nitrone Derivatives
Authors	George Baffour Pipim, Richard Tia and Evans Adei
Publication Date	08 Apr. 2021
Article Type	Full Research Paper
Supporting Information File 1	SI BJOC.docx; 127.6 KB
ORCID® iDs	George Baffour Pipim - https://orcid.org/0000-0002-4700-8005; Richard Tia - https://orcid.org/0000-0003-1043-8869

Quantum Chemical Investigation of the Formation of Spiroheterocyclic Compounds Via the (3 + 2) Cycloaddition Reaction of 1-methyl-3-(2,2,2-trifluoroethylidene)pyrrolidin-2-one with Diazomethane and Nitrone Derivatives

George Baffour Pipim, Richard Tia* and Evans Adei

Theoretical and Computational Chemistry Laboratory, Department of Chemistry, Kwame Nkrumah University of Science and Technology, Kumasi, Ghana

baffourgeorge88@gmail.com, richardtia.cos@knust.edu.gh/ richtiagh@yahoo.com, eadei@yahoo.com

Abstract

Spirocycles are important structures in drug development due to their inherent biological activity. Their complex architecture usually presents many synthetic difficulties which are efficiently resolved with detailed theoretical studies. The chemo-, regio- and stereoselectivities of the formation of spiroheterocyclic compounds via the (3 + 2) cycloaddition (32CA) reaction of 1-methyl-3-(2,2,2-trifluoroethylidene)pyrrolidin-2-one (**A1**) derivatives with diazomethane and nitrone derivative have been studied at the M06-2X/6-311G(d,p) level of theory. The reactions of diazomethane (**A2**) and *N*-methyl-*C*-phenyl nitrone (**A3**) derivatives with 1-methyl-3-(2,2,2-trifluoroethylidene)pyrrolidin-2-one derivatives (**A1**) occurs chemoselectively along the olefinic bond of **A1** via an asynchronous one-step mechanism. Analysis of the electrophilic (P_K^+) and nucleophilic (P_K^-) Parr functions at the different reaction sites in **A1** shows that **A2** and **A3** add across the atomic centers with the largest Mulliken and NBO atomic spin densities. Both electron-donating groups (EDGs) and electron-withdrawing groups (EWGs) on the **A3** molecule do not affect the observed preferred pathway in its 32CA reaction with **A1** whereas the electronic and steric nature of the substituent on the **A2** molecule influences the preferred pathway in the 32CA reaction of **A1** and **A2**. The title reaction proceeds via forward electron denisity flux (FEDF), where electron density fluxes from the three-atom components (**A2** and **A3**) to **A1**. The computed global electron density transfer (GEDT) values suggest that the 32CA of **A1** with diazomethane is a polar reaction while the 32CA reaction of **A1** with *N*-methyl-*C*-phenyl nitrone is a non-polar reaction, and an inverse relationship has been established between the polar character of the reactions and activation barriers. In all the reactions studied, the selectivities are kinetically controlled.

1.0   Introduction

Spirocyclic compounds are molecular rings sharing a common atom; the simplest of these being bicyclic compunds. Their fascinating molecular framework and their presence in a variety of natural products are of special interest to chemists [1–8]. Within a three-dimensional fragment space, spirocycles are an essential class of molecular ring systems [5,9,10]. Their quaternary atomic center avails an inherent three-dimensionality to this class of scaffolds whereas their cyclic nature provides all the benefits of reduced flexibility. These characteristics are largely responsible for their biological activity [9,11,12]. Over the years, many synthetic procedures have been developed to construct spirocycles, most of which are usually based on cycloaddition reactions or condensation reactions [13]. The construction of a spirocyclic framework commonly involves the formation of a new ring on an existing ring system [1]. Synthesis of spiroheterocycles is particularly challenging; however, they present an under-explored area of the chemical library with outstanding potential in drug design [9].

Cycloaddition reactions are important synthetic procedures for the transformation of both cyclic and acyclic precursors into complex spirocyclic compounds [14]. The (3 + 2) cycloaddition (32CA) reaction of three-atom components (TACs) and ethylene derivatives presents convenient methods to access spiroheterocyclic compounds of valuable pharmacological and therapeutic properties [1,15–18]. The major challenge in the application of the 32CA reaction is to control the regio-, stereo-, and enantio-selectivities [19,20]. The stereochemistry of the 32CA reaction can be controlled by either employing   the appropriate substrates or controlling the reaction with a catalyst.

Diazomethane and its derivatives are versatile TAC for constructing spiroheterocycles. Padwa and Goldstein reported a 32CA between diazoindene and electron-deficient acetylenic and ethylene derivatives [21]. They reported that the formation of the spiro-3*H*-pyrazole cycloadduct was dependent on the substituents on the reagents and the formed cycloadduct can lose nitrogen to furnish spirocyclopropane [21]. Work by Cheng et al. [22] showed an efficient route to spiro-3*H*-indazoles bearing a carbonyl group adjacent to the spiro carbon via 32CA reaction of arynes with 6-diazocyclohex-2-en-1-one derivatives.

The formation of a spiroheterocycle containing an isoxazolidine ring structure is achieved conveniently by employing the 32CA reaction of nitrones . Jegham et al. reported a regio- and stereo-selective synthesis of spiro-isoquinolinediones from the reaction of (*E*)-4-arylidene-N-methyl-isoquinoline-1,3-dione derivatives with *C*-aryl-*N*-phenylnitrones. They reported that the observed regiochemistry was dependent on the electronic nature of substituents on the (*E*)-4-arylidene-N-methyl-isoquinoline-1,3-dione derivatives [23]. Goti and co-workers described the diastereoselective synthesis of 5-spirosubstituted isoxazolidines via the 32CA reaction of *C,N*-diphenylnitrone with methylenebutyrolactones and the observed diastereoselectively was controlled by steric effects in the transition states [24].

Bouillon et al. [25] described an efficient synthesis of spiroheterocycles via the 32CA reaction of 1-methyl-3-(2,2,2-trifluoroethylidene)pyrrolidin-2-one derivatives (**A1**) with diazomethane (**B2**) and *N*-methyl-*C*-phenyl nitrone (**B3**) (see scheme 1). The reaction of **A1** (R_1 = H) with **B2** chemo- and regio-selectively generated the spirocyclic pyrazoline **1** in good yield. Spirocycloadduct **2** was formed as the major product from the reaction of **A1** (R_1 = H) with **B3** whereas the 32CA reaction of **A1** (R_1 = OH) with **B3** yielded **3** [25] as the major product. The generated spiroheterocycles present great relevance in contemporary synthetic and pharmaceutical chemistry. The molecular

mechanism, substrate reactivity, and factors controlling the chemo-, regio- and stereoselectivities involved in this reaction remains unknown.
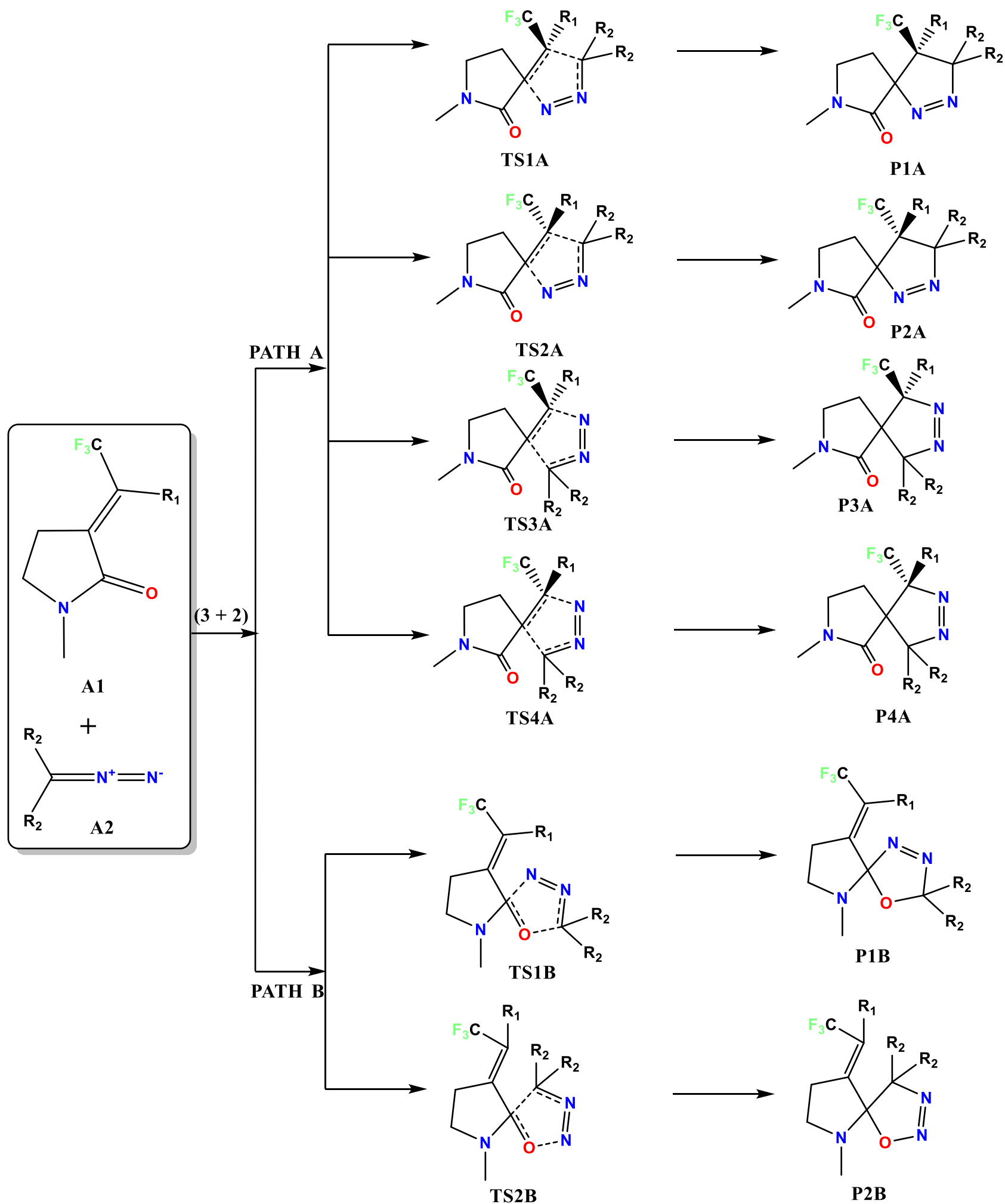
Scheme 1: 32CA reaction of of 1-methyl-3-(2,2,2-trifluoroethylidene)pyrrolidin-2-one derivatives (**A1**) with diazomethane (**B2**) and *N*-methyl-*C*-phenylnitrone (**B3**)
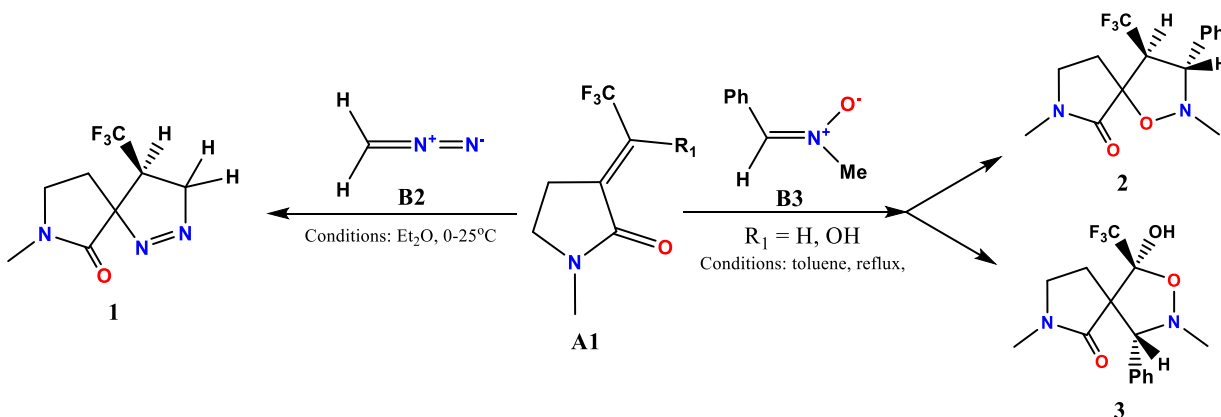
We report for the first time, a detailed theoretical study on the chemo-, regio- and stereo-selectivities of the 32CA reactions of 1-methyl-3-(2,2,2-trifluoroethylidene)pyrrolidin-2-one derivatives (**A1**) with diazomethane (**A2**) (see scheme 2) and *N*-methyl-*C*-substituted nitrone derivatives (**A3**) (see scheme 3). The mechanistic effect of substituents, as well as solvents on the reactions, have been investigated.

Scheme 2: Proposed scheme of study for the 32CA reaction of 1-methyl-3-(2,2,2-trifluoroethylidene)pyrrolidin-2-one derivatives (**A1**) with diazomethane (**A2**)

Scheme 3: Proposed Scheme of Study for the 32CA reaction of 1-methyl-3-(2,2,2-trifluoroethylidene)pyrrolidin-2-one one derivatives (**A1**) with *N*-methyl-*C*-substituted nitrone derivatives (**A3**)
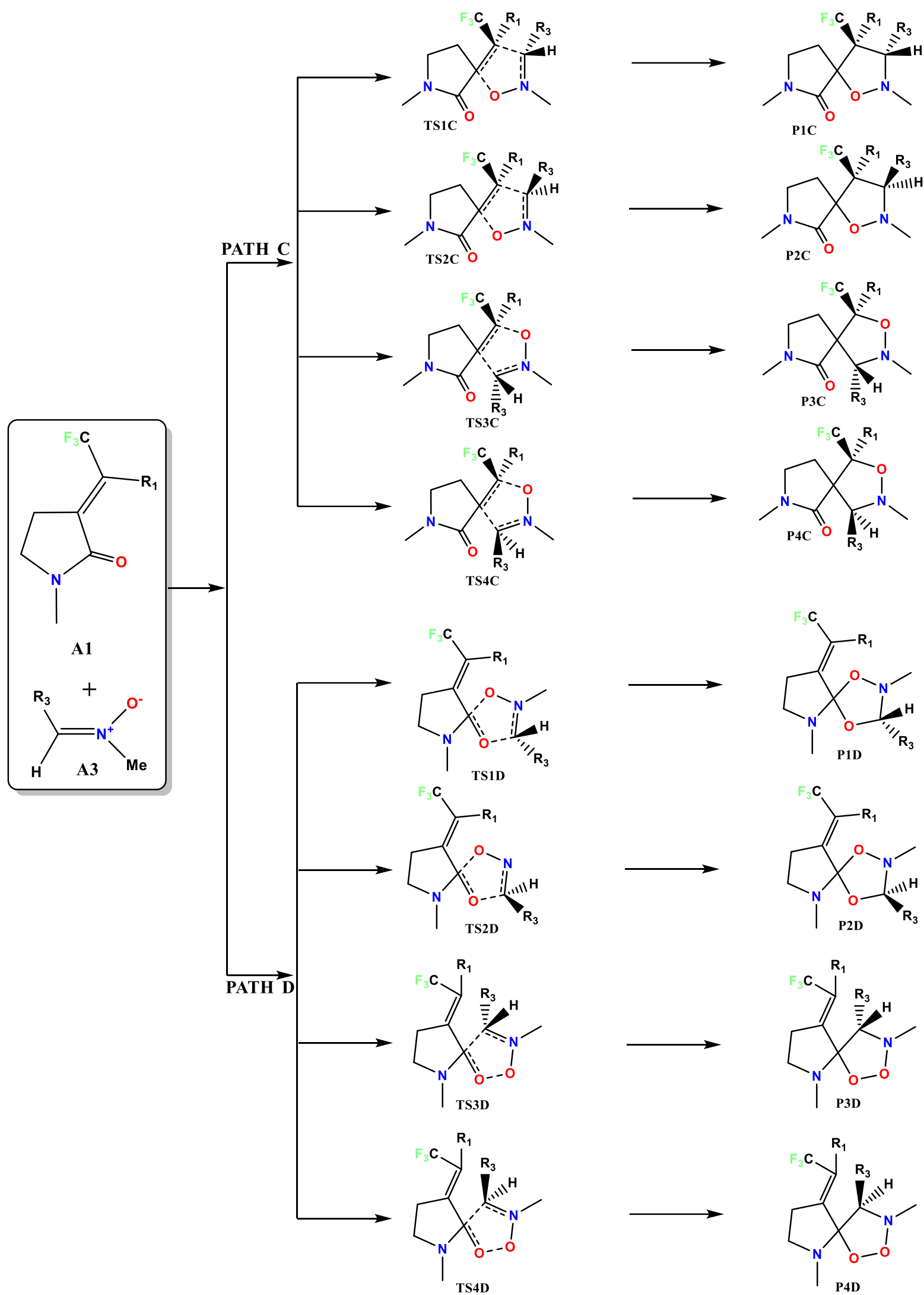
2.0 Computational Details and Methodology

All quantum chemical calculations were performed using Gaussian '09 [26] and Spartan 14 [27] computational chemistry software suites at the M06-2X/6-311G(d,p) level of theory. The M06-2X functional [28] has been established to be effective at computing thermochemistry and kinetics of reactions [29–31]. In the Minnesota hybrid meta-generalized gradient approximations (meta-GGA) set of density functionals, M06-2X is among the best performing in geometry optimizations and energy calculations [32]. Some recent studies on selected organic reactions have established the M06-2X coupled with the 6-311G(d,p) level of theory as the best choice as it avoids higher energetic barriers associated with, for instance, B3LYP [33,34]. To further test the suitability of the level of theory chosen, the parent reactions were also computed (full geometry optimization and energy calculations) at the M06-2X-D3/6-311G(d,p), M06-2X-D3/6-311++G(d,p), M06/6-311++G(d,p), M06-D3/6-311++G(d,p), B3LYP-D3/6-311++G(d,p) and B3LYP-D3/6-311G(d,p) level of theory for comparison.

Guess structures of all the considered molecules were constructed using the Spartan 14 [27] graphical model builder and minimized interactively using the sybyl force field.[35] Transition state structures were computed by first obtaining guess input structures by constraining specific internal coordinates of the molecules (bond lengths, bond angles, dihedral angles) while fully optimizing the remaining internal coordinates. This procedure gives appropriate guess transition state input geometries which are then submitted for full transition state calculations without any geometry or symmetry constraints. Using the polarizable continuum model (PCM), diethyl ether was employed to compute solvation effects in the reactions.[36] The full optimization calculations were carried out with the Gaussian 09 package. Full harmonic vibrational frequency calculations were carried out to ensure that all transition state structures have a Hessian matrix with only a

single negative eigenvalue, characterized by an imaginary vibrational frequency along the respective reaction coordinates. Intrinsic reaction coordinate calculations were then performed to ensure that each transition state smoothly connects the reactants and products along the reaction coordinate.[33,34,37,38] The optimized structures were illustrated using CYLview.[39]

The global electrophilicity (ω) and maximum electronic charge (ΔN_{max}) of the various diazomethane derivatives were calculated using equations (1) and (2). The electrophilicity index measures the ability of a reactant to accept electrons [40] and is a function of the electronic chemical potential, $\mu = (E_{HOMO} + E_{LUMO})/2$ and chemical hardness, $\eta = (E_{LUMO} - E_{HOMO})$ as defined by Pearson's acid-base concept [41]. Hence, species with large electrophilicity values are more reactive towards nucleophiles. These equations are based on the Koopmans theory [42] originally established for calculating ionization energies from closed-shell Hartree–Fock wavefunctions but have since been adopted as acceptable approximations for computing electronic chemical potential and chemical hardness.

$$\omega = \mu^2/2\eta \qquad\qquad (1)$$
$$\Delta N_{max} = -\mu/\eta \qquad\qquad (2)$$

The maximum electronic charge transfer (ΔN_{max}) measures the maximum electronic charge that the electrophile may accept. Thus, species with the largest ΔN_{max} index would be the best electrophile given a series of compounds.

The electrophilic (P_K^+) and nucleophilic (P_K^-) Parr functions were obtained through the analysis of the Mulliken and Natural Bond Orbital (NBO) atomic spin densities (ASD) of the radical anion and the radical cation by single-point energy calculations over the optimized neutral geometries using the unrestricted UM06-2X formalism for the radical species [43]. The nucleophilicity index

of the various reagents was calculated using equation (3). This scale of nucleophilicity is referred to as tetracyanoethylene (TCE) [44].

$$N_{(nu)} = E_{HOMO(nu)}(eV) - E_{HOMO(TCE)}(eV) \qquad (3)$$

The global electron density transfer [45] (GEDT) was computed from the sum of the natural atomic charges, obtained by a natural population analysis (NPA) [46,47], of the atoms belonging to each framework at the transition states. The sign indicates the direction of the electron density flux in such a manner that positive values mean a flux from the considered framework to the other one.

The rate constants of the reaction at a given temperature [k(T)] for the (3 + 2) cycloaddition reaction of 1-methyl-3-(2,2,2-trifluoroethylidene)pyrrolidin-2-one derivatives with diazomethane and *N*-methyl-*C*-phenyl nitrone were calculated using equation (3) [48].

$$k(T) = \frac{K_B T}{hc°} \ e^{-\Delta^{\ddagger}G°/RT} \qquad (3)$$

where k_B = 1.380662 x 10^{-23} J/K is Boltzmann's constant, T = 298.15 K is the reaction temperature, h = 6.62617 x 10^{-34} J.s is Planck's constant, R = 1.987 cal/mol.K is the molar gas constant, $\Delta^{\ddagger}G°$ is the Gibbs free energy of activation,, and $c°$ is the concentration of the reacting species which is taken as 1.

3.0   Results and Discussion

We investigate the mechanism of the 32CA reaction of diazomethane derivatives (**A2**) with **A1** by exploring six different reaction channels that correspond to different chemo-, regio, and stereo-isomeric approach modes of **A2** to **A1** (scheme 2). The addition of the diazomethane derivatives (**A2**) across the olefinic bond in **A1** results in four regio- and stereo-isomeric products **P1A**, **P2A**, **P3A**, and **P4A** through transition states **TS1A**, **TS2A**, **TS3A**, and **TS4A** respectively.   The structural formula **P1A** and **P2A** are stereoisomers; likewise, **P3A** and **P4A** are stereoisomeric spirocycloadducts. Path B originates from the addition of the **A2** across the carbonyl group in **A1** to afford regioisomers **P1B** and **P2B** through **TS1B** and **TS2B**.

Due to the molecular asymmetry of the reactants in scheme 3, eight reaction routes have been considered for the 32CA reaction of *N*-methyl-*C*-substituted nitrone (**A3**) with **A1**. **P1C**, **P2C**, **P3C**, and **P4C** arise from the addition of the nitrone across the olefinic bond in **A1** through **TS1C**, **TS2C**, **TS3C,** and **TS4C** respectively. **P1C** and **P2C** are diastereomers; similarly, **P3C** and **P4C** are diastereomers. The addition of the nitrone across the carbonyl functionality of **A1** affords four isomeric spirocycloadducts **P1D**, **P2D**, **P3D**, and **P4D** through transition states **TS1D**, **TS2D**, **TS3D**, and **TS4D**. **P1D** and **P2D** are diastereomers and **P3D** and **P4D** are also diastereomeric pairs.

The present study has been divided into two major parts: (i) first, we analyze the 32CA reaction of (E)-1-methyl-3-(2,2,2-trifluoroethylidene)pyrrolidin-2-one (**A1** = H) with diazomethane derivatives (**A2**) given in scheme 2 (ii) next, we examine the 32CA reaction of 1-methyl-3-(2,2,2-trifluoroethylidene)pyrrolidin-2-one derivatives (**A1** = H, OH) with *N*-methyl-*C*-substituted nitrone (**A3**).

3.1.1 Study of the Competitive Pathways Associated with the 32CA Reaction of (E)-1-methyl-3-(2,2,2-trifluoroethylidene)pyrrolidin-2-one with Diazomethane

The mechanistic details of the 32CA reaction of (E)-1-methyl-3-(2,2,2-trifluoroethylidene)pyrrolidin-2-one (**A1**, R_1 = H) and diazomethane (**A2**, R_2 = H) have been examined in this section. The activation and reaction energies of the six reaction pathways obtained from gas phase computations at the M06-2X/6-311G level of theory have been shown graphically in figure 1. The activation and reaction energies for the 32CA reaction of **A1** (R_1 = H) and **A2** (R_2 = H) for solvent phase (diethyl ether) computations are shown in parenthesis in figure 1.

Some interesting conclusions can be drawn from the gas-phase energies displayed in figure 1: (a) the addition is highly chemoselective towards the exocyclic olefinic bond of **A1** (R_1 = H) to afford the corresponding spiropyrazoline cycloadducts. (b) the activation energies associated with the addition of **A2** (R_2 = H) across the olefinic bond of **A1** (R_1 = H) range from 7.2 kcal/mol to 16.0 kcal/mol with the most favorable reaction path regioselectively leading to the formation of **P1A** through **TS1A** with an activation energy of 7.2 kcal/mol. The formation of **P1A** is highly exergonic with reaction energy of -37.0 kcal/mol. Its respective diastereomer (**P2A**) proceeds through **TS2A** with a higher activation energy of 13.6 kcal/mol. Likewise, the formation of **P3A** is kinetically favored over its respective diastereomer **P4A** by an energy barrier of 5.3 kcal/mol. (c) relatively higher activation barriers are observed for reaction along the carbonyl group of **A1** (R_1 = H) and the resulting spirocycloadduct are thermodynamically unstable. (d) the reaction is kinetically controlled. From figure 1, negligible variation in both activation and reaction energies is observed for solvent phase computation. The energetic trends observed remain the same as in the gas phase computation.

The polar character of the competitive reaction paths has been investigated by calculating the GEDT at the four transition states (**TS1A**, **TS2A, T3A**, and **TS4A**) associated with the addition of the diazomethane **A2** (R_2 = H) across the exocyclic olefinic bond of **A1** (R_1 = H). Reactions with GEDT values of 0.0 e correspond to non-polar processes, while values higher than 0.2 e correspond to polar processes [1,45]. The 32CA reaction of **A2** (R_2 = H) along the olefinic bond of **A1** (R_1 = H) proceeds via a forward electron density flux (FEDF) [49,50] . Thus electron density fluxes from **A2** (R_2 = H) to **A1** (R_1 = H). The GEDT, which fluxes from **A2** (R_2 = H) to **A1** (R_1 = H) is 0.47 e at **TS1A**, 0.21 e at **TS2A**, 0.22 e at **TS3A**, and 0.20 e at **TS4A**. An inverse relationship exists between the GEDT values and the activation barriers. The GEDT values indicate the highest polar character at **TS1A** which is consistent with the height of its activation barrier.

The optimized transition state structures of all the reaction routes considered in scheme 2 for the 32CA reaction of **A1** (R_1 = H) and **A2** (R_2 = H) for both gas and solvent phases are shown in figure 2. Evident from figure 2, diazomethane is distorted from its linear reactant geometry to achieve its transition state geometry. The observed activation energies can partly be attributed to the distortion energies [51] of the diazomethane. An asynchronous one-step mechanism is observed for the addition of the diazomethane across **A1** (R_1 = H). In all the pathways considered for the reaction of **A2** (R_2 = H) along the exocyclic olefinic bond, the formation of the carbon-carbon bonds are more advanced in the transition states than the carbon-nitrogen bonds. The study of the geometric parameters of the transition states structures obtained for the gas and solvent phase computations in figure 2 shows that the inclusion of diethyl ether solvation in the computations does not substantially change the geometrical parameters.
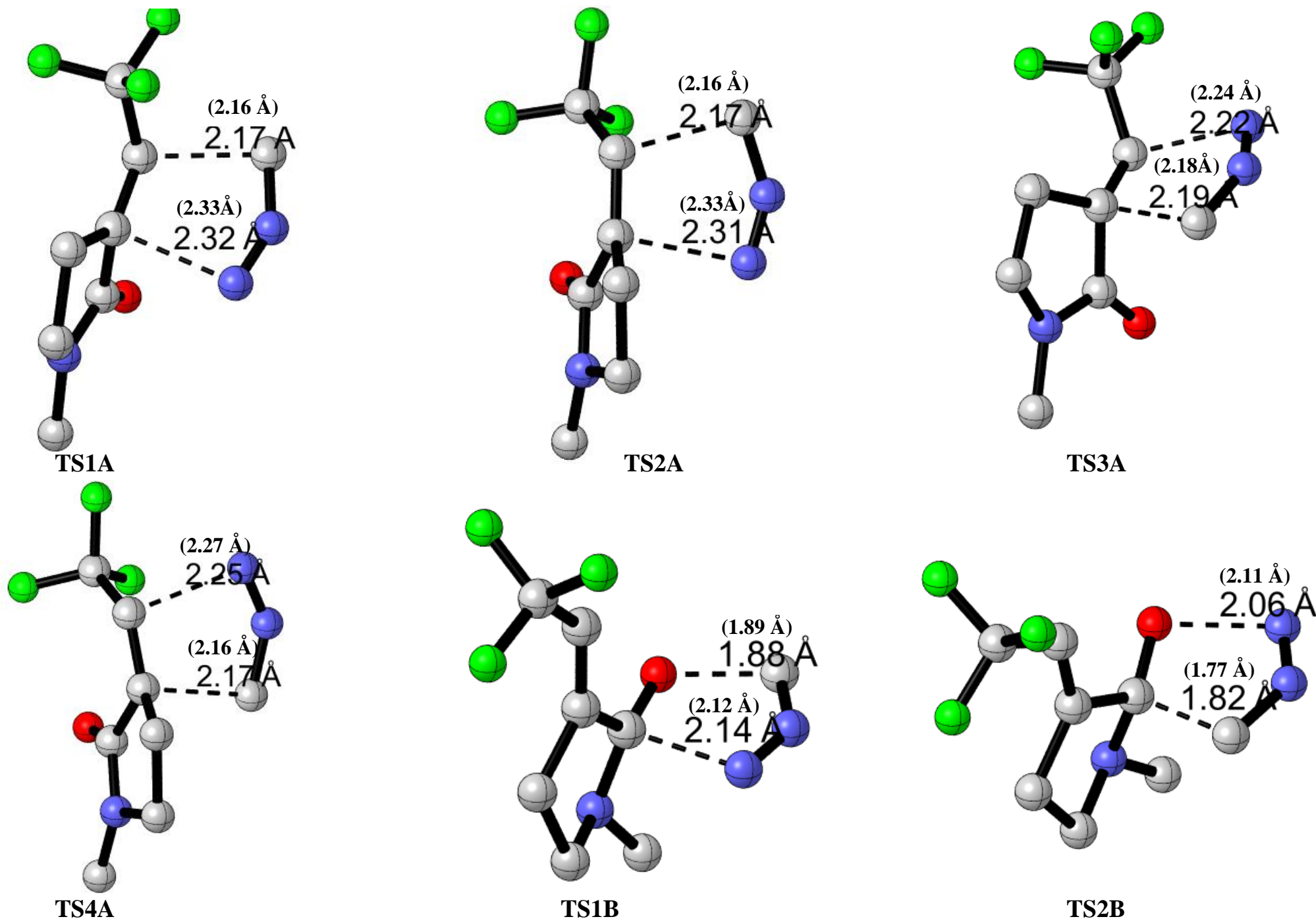
The rate constants for the formation of the six chemo-, regio- and stereoisomeric spirocycloadducts considered for the 32CA reaction of **A1** (R_1 = H) and **A2** R_2 = H) at the M06-2X/6-311G M06-

2X/6-311G(d,p) level of theory in the gas phase have been calculated and the results displayed in table 1. The highest calculated rate constant is $3.3 \times 10^7\,\text{s}^{-1}$ and its associated with the formation of **P1A** via **TS1A**. This is consistent with the high yields of **P1A** observed experimentally by Bouillon et al. [25]. The closest competing path leads to **P3A** at a rate about 370 times slower than the formation of **P1A**. The rate constants shown in table 2 suggest a clear cut selectivity between the various diastereomers. Thus **P1A**, **P3A**, and **P1B** are selective over their diastereomers **P2A**, **P4A**, and **P2B** respectively.

To investigate the possibility of the M06-2X/6-311G(d,p) level of theory considerably underestimating the activation barriers, the reaction of 32CA reaction of **A1** (R_1 = H) and **A2** (R_2 = H) were re-computed (full optimizations and not just single-point energy calculations) with different functionals, and the results, as shown in table 2, indicate that the difference in barriers between the methods is within ± 3 kcal/mol. Thus, compared to the other levels of theory, the activation barriers of M06-2X/6-311G(d,p) are realistic for the reactions under study.
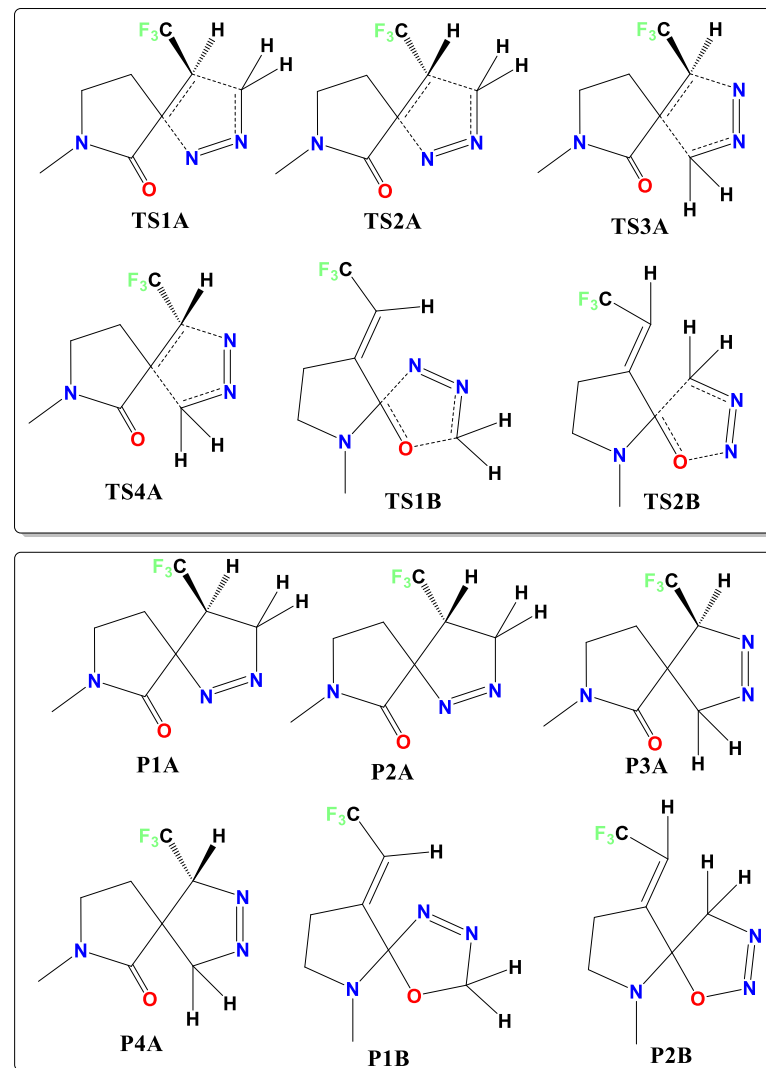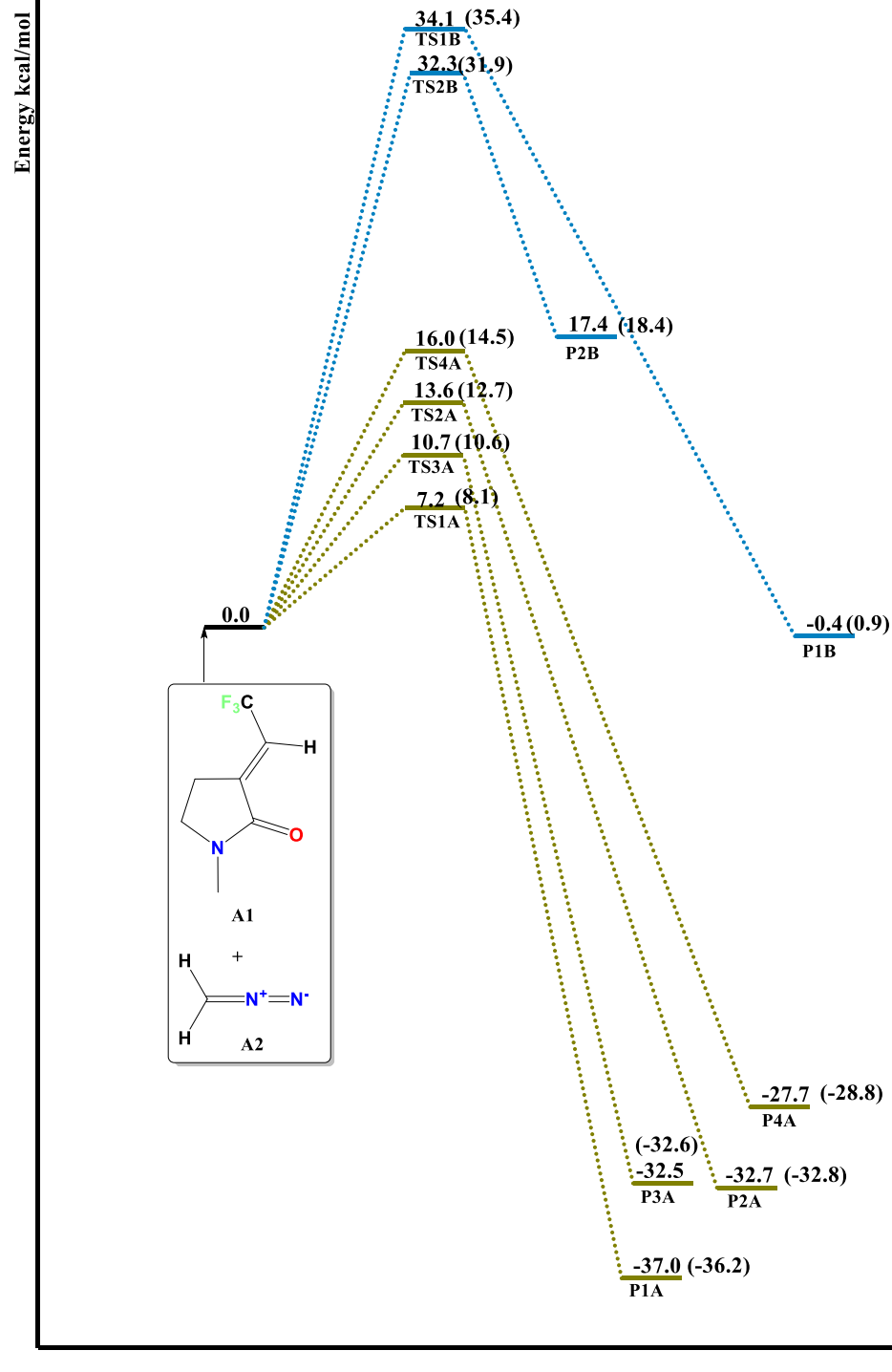
Figure 1: Gibbs free energy profile for the 32CA reaction of **A1** (R_1 = H) and **A2** (R_2 = H) at the M06-2X/6-311G(d,p) level of theory in the gas-phase. Energies observed in the solvent-phase (diethyl ether) computations at M06-2X(PCM)/6-311G (d,p), level of theory are shown in parentheses.

Figure 2: Optimized transition state structures involved in the six chemo-, regio-, and diastereoisomeric reaction paths considered for the 32CA reaction of **A1** (R_1 = H) and **A2** (R_2 = H) at the M06-2X/6-311G M06-2X/6-311G(d,p) level of theory in the gas-phase. All labeled bond distances are in Angstrom (Å). Distances in diethyl ether solvation are given in parentheses. All hydrogens have been omitted to ensure the simplicity of structures.

Table 1: Rate constants (in s^{-1}) at 25°C for the 32CA reaction of **A1** (R$_1$ = H) and **A2** (R$_2$ = H) at the M06-2X/6-311G M06-2X/6-311G(d,p) level of theory in the gas phase.

Product	Rate constants (k[T])
P1A	3.3×10^7
P2A	6.7×10^2
P3A	8.9×10^4
P4A	1.2×10^1
P1B	1.3×10^{-11}
P2B	6.2×10^{-13}

Table 2: Activation energies of the six pathways considered for 32CA reaction of **A1** (R$_1$ = H) and **A2** (R$_2$ = H) at different levels of theory in the gas phase. All energies are in kcal/mol.

| LEVEL OF THEORY	TS1A	TS2A	TS3B	TS4A	TS1B	TS2B
M06-2X/6-311G (d,p)	7.2	13.6	10.7	16.0	34.1	32.3
M06-2X-D3/6-311G (d,p)	6.9	13.2	10.3	15.7	33.8	32.0
M06-2X-D3/6-311++G (d,p)	7.9	14.4	11.2	16.6	33.8	32.2
M06/6-311++G (d,p)	9.4	15.9	13.3	18.5	36.1	33.9
M06-D3/6-311++G (d,p)	8.0	14.6	11.9	17.1	34.6	32.7
B3LYP-D3/6-311G (d,p)	7.9	14.4	12.1	17.4	33.8	33.0
B3LYP-D3/6-311++G (d,p)	9.3	16.0	13.3	18.8	33.8	34.5

3.1.2 Analysis of the Origin of Chemo- and Regioselectivities observed in the 32CA Reaction of (E)-1-methyl-3-(2,2,2-trifluoroethylidene)pyrrolidin-2-one with Diazomethane with Local Reactivity Indices

The local electrophilic (P_K^+) and nucleophilic (P_K^-) Parr functions have been employed to rationalize the chemo- and regioselectivities observed in the 32CA reaction of (E)-1-methyl-3-(2,2,2-trifluoroethylidene)pyrrolidin-2-one (**A1**, R_1 = H) and diazomethane (**A2**, R_2 = H) and the results are shown in table 3. Figure 4 is a graphical illustration of the atomic labels of **A1** (R_1 = H) and **A2** (R_2 = H). Both the Mulliken and NBO atomic spin densities (ASD) analyses have been employed to examine the source of chemo- and regioselectivities. These analyses provide a quantitative measure of the electron density at the various atomic centers within a molecule. Within the **A1** (R_1 = H), atomic centers with the largest electron density are the ideal point of attachment by the **A2** (R_2 = H) molecule.

From the table 3, with regards to the electrophilic Mulliken spin densities, analysis of the reaction sites in the **A1** (R_1 = H) shows that C_2 = 0.427, C_3 = 0.201, C_7 = 0.117 and O_1 = 0.149. The relatively large electron density present at C_2 and C_3 compared to C_7 and O_1 accounts for the chemoselective addition of the **A2** (R_2 = H) across the exocyclic olefinic bond of **A1** (R_1 = H). A similar pattern is observed for the analysis of the reaction centers in the **A1** (R_1 = H) with the NBO atomic spin density.

With regards to the nucleophilic Mulliken spin densities of the **A2** (R_2 = H) molecule, C_8 = -0.107 and N_3 = 0.707 as shown in table 3. The electrophilic C_8 atom prefers to bind to the comparatively nucleophilic C_2 atom whereas the nucleophilic N_2 prefers to bind to the relatively electrophilic C_3 atom in the addition of the **A2** (R_2 = H) across the exocyclic olefinic bond in **A1** (R_1 = H). This preferential attachment of atoms selectively leads to the formation of **P1A** over **P3A**, and **P2A**

over **P4A**, which is in total agreement with the regioselectivities observed. A similar trend is observed for the analysis with NBO atomic spin density.
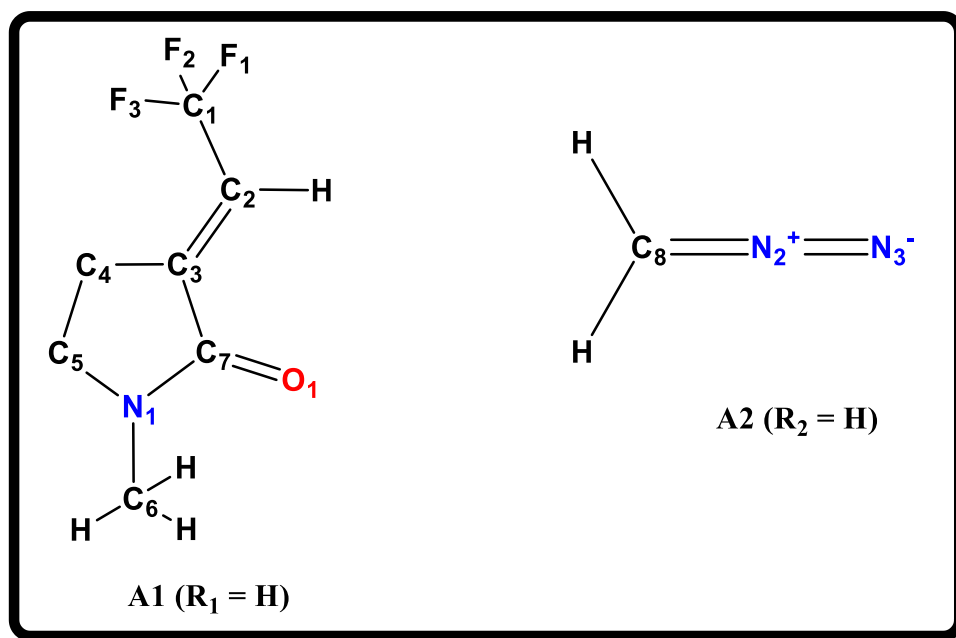
Figure 3: Atomic labels of (E)-1-methyl-3-(2,2,2-trifluoroethylidene)pyrrolidin-2-one (**A1**, R_1 = H) and diazomethane (**A2**, R_2 = H)

Table 3: Mulliken and NBO atomic spin densities of (E)-1-methyl-3-(2,2,2-trifluoroethylidene)pyrrolidin-2-one (**A1**, R_1 = H) and diazomethane (**A2**, R_2 = H)

| | **A1** (R_1 = H) NBO | | | **A2** (R_2 = H) NBO | | | **A1** (R_1 = H) MULLIKEN | | | **A2** (R_2 = H) MULLIKEN | |
	ANION	CATION		ANION	CATION		ANION	CATION		ANION	CATION
C_1	-0.001	0.044	C_8	-0.092	0.820	C_1	-0.003	0.049	C_8	-0.107	0.859
C_2	0.027	0.395	N_2	0.276	-0.152	C_2	0.033	0.427	N_2	0.260	-0.192
C_3	-0.0	0.199	N_3	0.694	0.392	C_3	-0.002	0.201	N_3	0.707	0.410
C_4	0.004	-0.012				C_4	0.01	-0.030			
C_5	0.014	0.002				C_5	0.052	0.021			
C_6	-0.011	0.0				C_6	0.034	-0.003			
C_7	-0.088	0.117				C_7	-0.097	0.117			
O_1	0.140	0.154				O_1	0.144	0.149			
N_1	0.739	0.032				N_1	0.766	0.023			
F1	0.001	0.003				F1	0.001	0.001			
F2	0.001	0.023				F2	0.001	0.016			
F3	-0.0	0.014				F3	-0.0	0.009			

3.1.3 Analysis of the 32CA Reaction of (E)-1-methyl-3-(2,2,2-trifluoroethylidene)pyrrolidin-2-one with Diazomethane Derivatives

In this segment, we examine the mechanistic effects of different substituents on the diazomethane molecule in its reaction with (E)-1-methyl-3-(2,2,2-trifluoroethylidene)pyrrolidin-2-one (**A1**, R_1 = H). Table 4 shows the results for the 32CA reaction of diazomethane derivatives and **A1** (R_1 = H). Some conclusions can be drawn from the results displayed in table 4: (a) relative to the 32CA reaction of **A1** (R_1 = H) and **A2** (R_2 = H) at the M06-2X/6-311G M06-2X/6-311G(d,p) level of theory in the gas phase, the lower activation barriers are observed for the reaction of EDGs-substituted diazomethane (**A2**, R_2 = methyl, ethyl, cyclopropyl) with **A1** (R_1 = H) (b) while the formation of **P1A** is the most kinetically favorable reaction route among the six chemo-, regio- and diastereoisomeric pathways for the reactions of methyl- and ethyl-substituted diazomethane (**A2**, R_2 = methyl, ethyl) with **A1** (R_1 = H), the reaction of cyclopropyl-substituted diazomethane (**A2**, R_2 = cyclopropyl) proceeds through **TS3A** to afford **P3A**. This observed change in regioselectivity in the reaction of **A2** (R_2 = cyclopropyl) with **A1** (R_1 = H) can be attributed partially to the less steric hindrance encountered in the formation of **P3A** over **P1A** (c) the reactions of EWGs-substituted diazomethane (**A2**, R_2 = bromo, chloro, cyano) with **A1** (R_1 = H) proceed to form **P3A** (d) relative to the 32CA reaction of **A1** (R_1 = H) and **A2** (R_2 = H), a decrease in activation energies is observed for the reaction of **A2** (R_2 = bromo, chloro) with **A1** (R_1 = H) while an increase is observed for the reactions of **A2** (R_2 = cyano) and **A1** (R_1 = H) (e) the formation of **P3A** is the preferred pathway in the reaction of **A2** (R_2 = phenyl) with **A1** (R_1 = H). Likewise, the observed regioselectivity can be partly attributed to the bulky nature of the phenyl (f) in all substituents studied, the most competitive reaction routes lead to the formation of **P1A** and **P3A** through **TS1A** and **TS3A** respectively (g) the reactions of **A1** (R_1 = H) with diazomethane derivatives are kinetically controlled.

Table 4: Activation and reaction energies of transition states and products respectively for the 32CA reaction of diazomethane derivatives and **A1** (R_1 = H) at the M06-2X/6-311G (d,p) level of theory in the gas phase. All energies are in kcal/mol.

SUBSTITUENT (R_2)	TS1A	TS2A	TS3A	TS4A	TS1B	TS2B	P1A	P2A	P3A	P4A	P1B	P2B
Hydrogen	7.2	13.6	10.7	16.0	34.1	32.3	-37.0	-32.7	-32.5	-27.7	-0.4	17.4
Methyl	1.1	8.8	4.3	10.3	21.5	27.0	-40.9	-38.0	-35.5	-30.2	-9.3	15.4
Ethyl	2.0	10.2	5.6	11.4	22.7	28.1	-36.8	-35.0	-31.2	-26.2	-8.4	19.4
Cyclopropyl	8.7	12.1	5.8	11.7	24.3	31.6	-39.0	-36.2	-34.2	-28.2	-6.6	18.5
Bromo	5.0	11.0	4.1	10.4	25.7	25.5	-41.7	-37.1	-39.0	-32.3	-14.3	12.5
Chloro	2.6	8.6	1.6	8.1	22.4	22.3	-46.3	-41.8	-43.9	-37.3	-18.7	8.0
Cyano	18.0	23.1	15.0	21.9	43.6	39.0	-24.2	-20.0	-22.8	-17.1	9.2	28.6
Phenyl	8.9	18.6	6.2	16.7	21.7	41.9	-29.6	-25.7	-23.0	-15.1	-2.2	20.7

3.1.4 Global Reactivity Indices Analysis of the 32CA Reaction of (E)-1-methyl-3-(2,2,2-trifluoroethylidene)pyrrolidin-2-one with Diazomethane Derivatives

In this segment, we employ various conceptual tools to examine the 32CA reaction of (E)-1-methyl-3-(2,2,2-trifluoroethylidene)pyrrolidin-2-one (**A1**, R_1 = H) with diazomethane derivatives (**A2**). The electronic chemical potential (μ), chemical hardness (η), global electrophilicity (ω), maximum electronic charge transfer (ΔN_{max}) and nucleophilicity values (N) of the various diazomethane derivatives (**A2**) have been calculated and the results displayed in tables 5. The μ for **A1** (R_1 = H) is -4.55 eV and that of **A2** (R_2 = H) is -3.65eV hence a polar character is expected in the reaction of **A1** (R_1 = H) with **A2** (R_2 = H). This observation is consistent with the calculated GEDT values of the four competitive 32CA reaction pathways discussed in section 3.1.0.

Evidently from table 5, EDGs on the diazomethane (**A2**, R_2 = methyl, ethyl, cyclopropyl) increase the electronic chemical potential values relative to **A2** (R_2 = H), thus making the diazomethane derivatives strong electron-donating molecules. A similar observation is made for the phenyl-substituted diazomethane molecule (**A2**, R_2 = phenyl). Contrary to EDGs, EWGs on the diazomethane molecule (**A2**, R_2 = bromo, chloro, cyano) decreases the μ values relative to **A2** (R_2 = H) hence making the diazomethane derivatives strongly electron-acceptor molecules. While the reactions of **A1** (R_1 = H) with EDGs-substituted diazomethane are expected to present a more polar character, the reactions of EWGs-substituted diazomethane are expected to have a low polar character. The order of the electronic chemical potential for the various substituents on the diazomethane **A2** is given in the order cyano < chloro < bromo < hydrogen < phenyl < cyclopropyl < methyl < ethyl.

The global electrophilicity (ω) [40] and maximum electronic charge transfer (ΔN_{max}) [52] are convenient tools used in the analysis of the reactivity of species participating in polar organic reactions. The electrophilicity (ω) scale allows the classification of organic molecules as strong

electrophiles with $\omega > 1.5$ eV, moderate electrophiles with $\omega > 0.8$ eV and nucleophiles (marginal electrophiles) with $\omega < 0.8$ eV. The diazomethane molecule (**A2**, $R_2 = H$) is a moderate electrophile with a ω value of 0.87 eV. From the results shown in table 5, EDGs on the diazomethane molecule significantly reduces the ω values whereas EWGs increase the ω values. A similar trend is observed for the analysis of the calculated ΔN_{max} values for the diazomethane derivatives.

The nucleophilicity values (N) [44] provided in table 5 shows that **A2** (R_2 = cyano) is the poorest nucleophile among the diazomethane derivatives with an N value of 0.25 eV, while **A2** (R_2 = phenyl) with an N value of 2.85 eV represents the best nucleophile. Relative to **A2** (R_2 = hydrogen), EDGs on the diazomethane molecules tend to increase the nucleophilicity value. In contrast to EDGs, EWDs on **A2** reduces the N value.

Table 5: Global reactivity indices for the various diazomethane derivatives (**A2**). Orbital energies are in eV.

SUBSTRATE (A2) R_2	HOMO	LUMO	μ	H	ω	ΔN_{max}	N
Hydrogen	-7.46	0.16	-3.65	7.62	0.87	0.48	1.91
Methyl	-6.65	0.48	-3.08	7.13	0.67	0.43	2.72
Ethyl	-6.62	0.49	-3.06	7.11	0.66	0.43	2.75
Cyclopropyl	-6.71	0.44	-3.14	7.15	0.69	0.44	2.66
Bromo	-7.52	-1.5	-4.51	6.01	1.69	0.75	1.85
Chloro	-7.67	-1.42	-4.54	6.24	1.66	0.73	1.70
Cyano	-9.11	-2.1	-5.61	7.01	2.24	0.80	0.25
Phenyl	-6.52	-0.29	-3.41	6.23	0.93	0.55	2.85
A1 ($R_1 = H$)	-8.56	-0.54	-4.55	8.01	1.29	0.57	0.81

3.2.1 Study of the Reactions Paths Associated with the 32CA Reaction of (Z)-1-methyl-3-(2,2,2-trifluoro-1-hydroxyethylidene)pyrrolidin-2-one and *N*-methyl-*C*-phenyl nitrone

Figure 4 shows the Gibbs free energy profile for the 32CA reaction of (Z)-1-methyl-3-(2,2,2-trifluoro-1-hydroxyethylidene)pyrrolidin-2-one (**A1**, R_1 = OH) with *N*-methyl-*C*-phenyl nitrone (**A3**, R_3 = Ph) in the gas phase at the M06-2X/6-311G level of theory. The mechanistic effect of toluene solvation on the 32CA reaction of **A1** (R_1 = OH) and **A3** (R_3 = Ph) has been investigated and the results indicated in parentheses in figure 4.

Some conclusions can be drawn from the gas phase results displayed in figure 4; (a) the 32CA reaction of **A1** (R_1 = OH) and **A3** (R_3 = Ph) is highly chemoselective. The addition of **A3** (R_3 = Ph) across the exocyclic olefinic bond of **A1** (R_1 = OH) proceeds with lower barriers relative to the reaction of **A3** (R_3 = Ph) along the carbonyl bond of **A1** (R_1 = OH) (b) the exergonic reaction that proceeds through **TS3C** with an activation energy of 3.5 kcal/mol to furnish **P3C** spirocycloadduct is the most kinetically favored pathway in all reaction routes considered for the 32CA reaction of **A1** (R_1 = OH) and **A3** (R_3 = Ph). The formations of **P1C** and **P4C** are the closest competing pathways with an activation energy of 5.6 kcal/mol through **TS1C** and **TS4C** respectively (c) the formation of **P2C** via **TS2C** is the least favored pathway in the addition of **A3** (R_3 = Ph) across the olefinic moiety of **A1** (R_1 = OH) (d) significant regioselectivity is observed for **P1C** over **P2C** and **P3C** over **P4C** (e) the reaction of **A3** (R_3 = Ph) along the carbonyl moiety of **A1** (R_1 = OH) is endergonic with activation energies ranging from 21.2 kcal/mol (**TS1D**) to 58.9 kcal/mol (**TS4D**). Evident from figure 4, the activation and reaction energies obtained for toluene solvation show negligible variation relative to the energies observed for the gas phase computations.

The polar character of the four competitive pathways considered for the addition of **A3** (R_3 = Ph) across the olefinic moiety of **A1** (R_1 = OH) has been investigated by calculating the GEDT at the

transition states (**TS1C**, **TS2C, T3C**, and **TS4C**). Reactions with GEDT values of 0.0 e are non-polar, while values higher than 0.2 e correspond to polar reactions [1,45]. Similar to the addition of **A2** (R_2 = H) across the olefinic bond of **A1** (R_1 = H), the 32CA reaction of **A3** (R_3 = Ph) along the olefinic bond of **A1** (R_1 = OH) proceeds via a FEDF [49,50]. Thus, electron density fluxes from **A3** (R_3 = Ph) to **A1** (R_1 = OH). The GEDT, which fluxes from **A3** (R_3 = Ph) to **A1** (R_1 = OH) is 0.01 e at **TS1C**, 0.03 e at **TS2C**, 0.08 e **TS3C**, and 0.07 e at **TS4C** which indicate a non-polar character in the reaction addition of **A3** (R_3 = Ph) across the olefinic bond of **A1** (R_1 = OH).
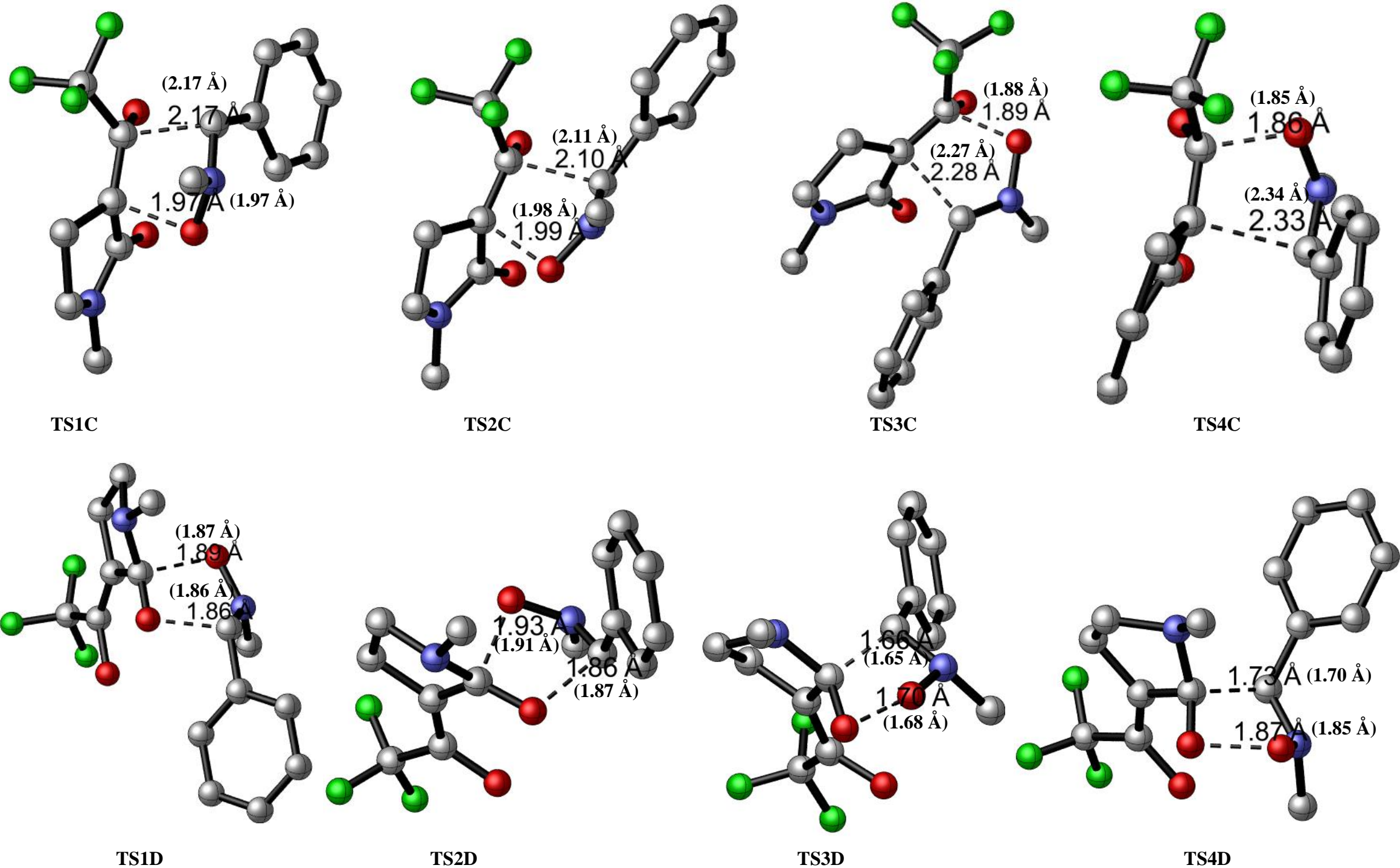
The optimized transition state structures with geometrical parameters of all the pathways considered in scheme 3 for the 32CA reaction of **A1** (R_1 = OH) and **A3** (R_3 = Ph) in both gas and solvent phases are shown in figure 5. An asynchronous one-step mechanism is observed for the addition of the **A3** (R_3 = Ph) across the reactive centers in **A1** (R_1 = OH). In all the pathways considered for the reaction of **A3** (R_3 = Ph) along the exocyclic olefinic bond of **A1** (R_1 = OH), the formation of the carbon-oxygen bonds is more advanced in the transition states than the carbon-carbon bonds. The study of the geometric parameters of the transition state structures for the gas and solvent phase computations in figure 5 shows that the inclusion of toluene solvation in the computations does not significantly change the geometries..

Table 5 shows the rate constants for the formation of all eight spirocycloadducts considered in scheme 3 for the 32CA reaction of **A1** (R_1 = OH) and **A3** (R_3 = Ph). The formation of **P3C** has the highest calculated rate constant of $1.7 \times 10^{10}\,\text{s}^{-1}$ which is in total agreement with the experimental yield of **P3C** reported by Bouillon et al. [25]. The closest competing pathways selectively proceed to afford **P1C** and **P4C** through **TS1C** and **TS4C** respectively with a rate constant of $4.9 \times 10^{8}\,\text{s}^{-1}$ which is approximately 35 times slower than the formation of **P3C**. The rate constants indicate a clear selectivity between the various diastereomers. This diastereoselectivity is more pronounced

in the formation of **P1C**, which is 7.7×10^8 times faster than the formation of its corresponding

diastereomer, **P2C**. The construction of **P1D** through **TS1D** (the most favorable reaction path for

the addition of **A3** (R_3 = Ph) across the carbonyl moiety of **A1** (R_1 = OH)) is 35000 times slower

than the formation of **P2C** (the least favorable pathway for the reaction of **A3** (R_3 = Ph) along the

olefinic bond of **A1** (R_1 = OH)) indicating clear chemoselectivity towards the addition across the

olefinic bond over the carbonyl bond of **A1** (R_1 = OH).
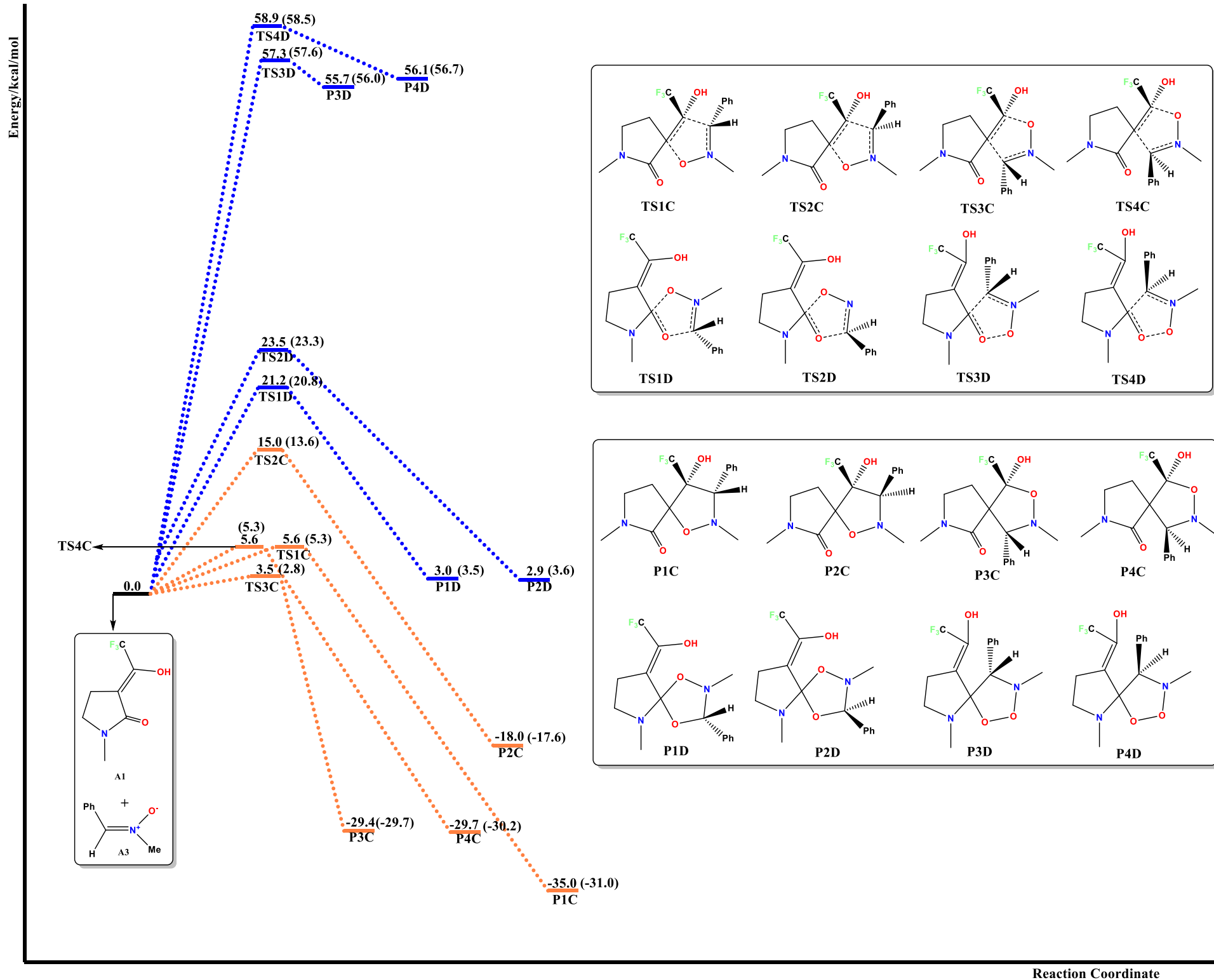
Figure 4: Gibbs free energy profile for the 32CA reaction of **A1** (R_1 = OH) and **A3** (R_3 = Ph) at the M06-2X/6-311G(d,p) level of theory in the gas-phase. Energies observed in the solvent-phase (toluene) computations at M06-2X(PCM)/6-311G (d,p), level of theory are shown in parentheses.

Figure 5: Optimized transition state structures involved in the eight chemo-, regio-, and diastereoisomeric reaction paths considered for the 32CA reaction of **A1** (R_1 = OH) and **A3** (R_3 = Ph) at the M06-2X/6-311G(d,p) level of theory in the gas-phase. All labeled bond distances are in Angstrom (Å). Distances in toluene solvation are given in parentheses. All hydrogens have been omitted to ensure the simplicity of structures.

Table 6: Rate constants (in s^{-1}) at 25°C for the 32CA reaction of **A1** (R_1 = OH) and **A3** (R_3 = Ph) towards the formation of the various products, computed at the M06-2X/6-311G M06-2X/6-311G(d,p) level of theory in the gas phase.

Product	Rate constants (k[T])
P1C	4.9×10^8
P2C	6.3×10^1
P3C	1.7×10^{10}
P4C	4.9×10^8
P1D	1.8×10^{-3}
P2D	3.7×10^{-5}
P3D	6.1×10^{-30}
P4D	4.1×10^{-31}

3.2.2 Study of the Competitive Pathways Associated with the 32CA Reaction of (E)-1-methyl-3-(2,2,2-trifluoroethylidene)pyrrolidin-2-one with *N*-methyl-*C*-phenyl nitrone

In this section, we examine the reaction of (E)-1-methyl-3-(2,2,2-trifluoroethylidene)pyrrolidin-2-one (**A1**, R_1 = H) with *N*-methyl-*C*-phenyl nitrone (**A3**, R_3 = Ph). Figure 6 shows the free energy profile for the 32CA reaction of **A1** (R_1 = H) and **A3** (R_3 = Ph) at the M06-2X/6-311G(d,p) level of theory in the gas phase. Toluene solvation effect on 32CA reaction of **A1** (R_1 = H) and **A3** (R_3 = Ph) has been investigated in the results shown in parentheses in figure 6.

The conclusions that can be drawn from the results displayed in figure 6 are; (a) similar to the reaction of **A1** (R_1 = OH) and **A3** (R_3 = Ph), the reaction of **A1** (R_1 = H) and **A3** (R_3 = Ph) is highly chemoselective towards the addition of the **A3** (R_3 = Ph) across the olefinic bond of **A1** (R_1 = H) (b) the formation of **P3C** through **TS3C** is the most kinetically favored pathway for the 32CA reaction of **A1** (R_1 = H) and **A3** (R_3 = Ph) in both gas and solvent phases. The reaction path that selectively leads to the formation of **P4C** is the closest competing with an activation energy of 5.0 kcal/mol (c) appreciable diastereoselectivity is observed for the formation of **P3C** over **P4C** whereas no diastereoselectivity is observed between **P1C** and **P2C** (d) the activation and reaction energies obtained for toluene solvation shows negligible variation relative to the energies observed for the gas phase computations.

The polar character of the four competitive pathways in the addition of **A3** (R_3 = Ph) across the olefinic moiety of **A1** (R_1 = H) has been examined by calculating the GEDT at the transition states (**TS1C**, **TS2C, T3C**, and **TS4C**). Similar to the 32CA reaction of **A3** (R_3 = Ph) along the olefinic bond of **A1** (R_1 = OH), the addition of **A3** (R_3 = Ph) across the olefinic moiety of **A1** (R_1 = H) proceeds via a FEDF [49,50]. The GEDT, which fluxes from **A3** (R_3 = Ph) to **A1** (R_1 = H) is 0.06 e at **TS1C**, 0.08 e at **TS2C**, 0.11 e **TS3C**, and 0.10 e at **TS4C** which indicate a non-polar character in the reaction addition of **A3** (R_3 = Ph) across the olefinic bond of **A1** (R_1 = H).

Evident from the labeled transition states bond distances in figure 7, the 32CA reaction of **A1** (R_1 = H) and **A3** (R_3 = Ph) proceed via an asynchronous one-step mechanism. Negligible structural differences were observed between the transition state structures obtained for gas and solvent phase computation.

Table 7 shows the rate constants for the formation of the eight chemo-, regio-, and diastereoisomeric spirocycloadducts considered in scheme 3 for the reaction of **A1** (R_1 = H) and **A3** (R_3 = Ph). Higher rate constants were obtained for the reaction of **A1** (R_1 = H) and **A3** (R_3 = Ph) relative to the reaction of **A1** (R_1 = OH) and **A3** (R_3 = Ph). The highest calculated rate constant (1.3×10^{11} s^{-1}) in table 7 is associated with the formation of **P3C** through **TS3C** which is approximately 8 times faster than the formation of **P3C** (the most favorable pathway) in the reaction of **A1** (R_1 = OH) and **A3** (R_3 = Ph).
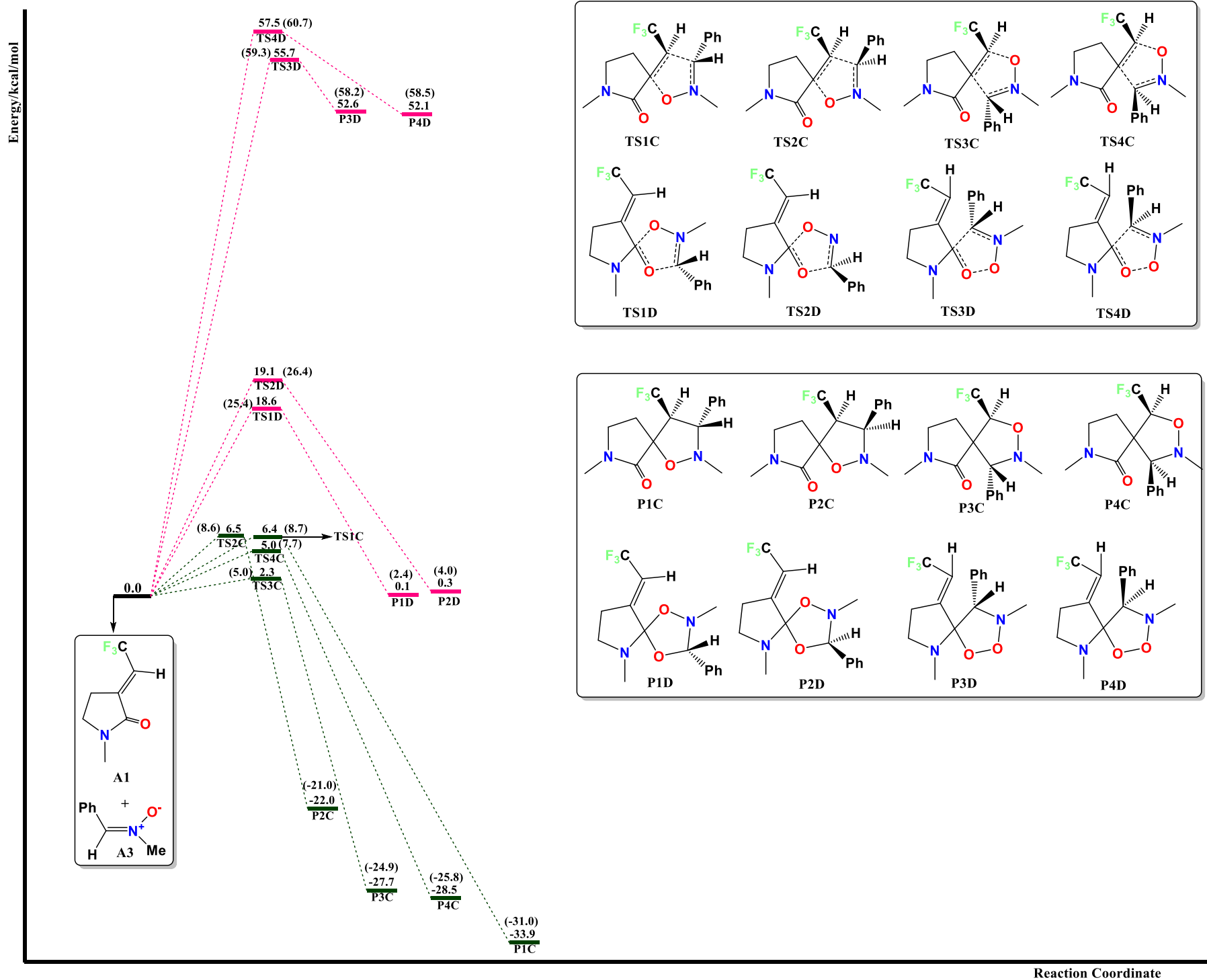
Figure 6: Gibbs free energy profile for the 32CA reaction of **A1** (R₁ = H) and **A3** (R₃ = Ph) at the M06-2X/6-311G(d,p) level of theory in the gas-phase. Energies observed in the solvent-phase (toluene) computations at M06-2X(PCM)/6-311G (d,p), level of theory are shown in parentheses.
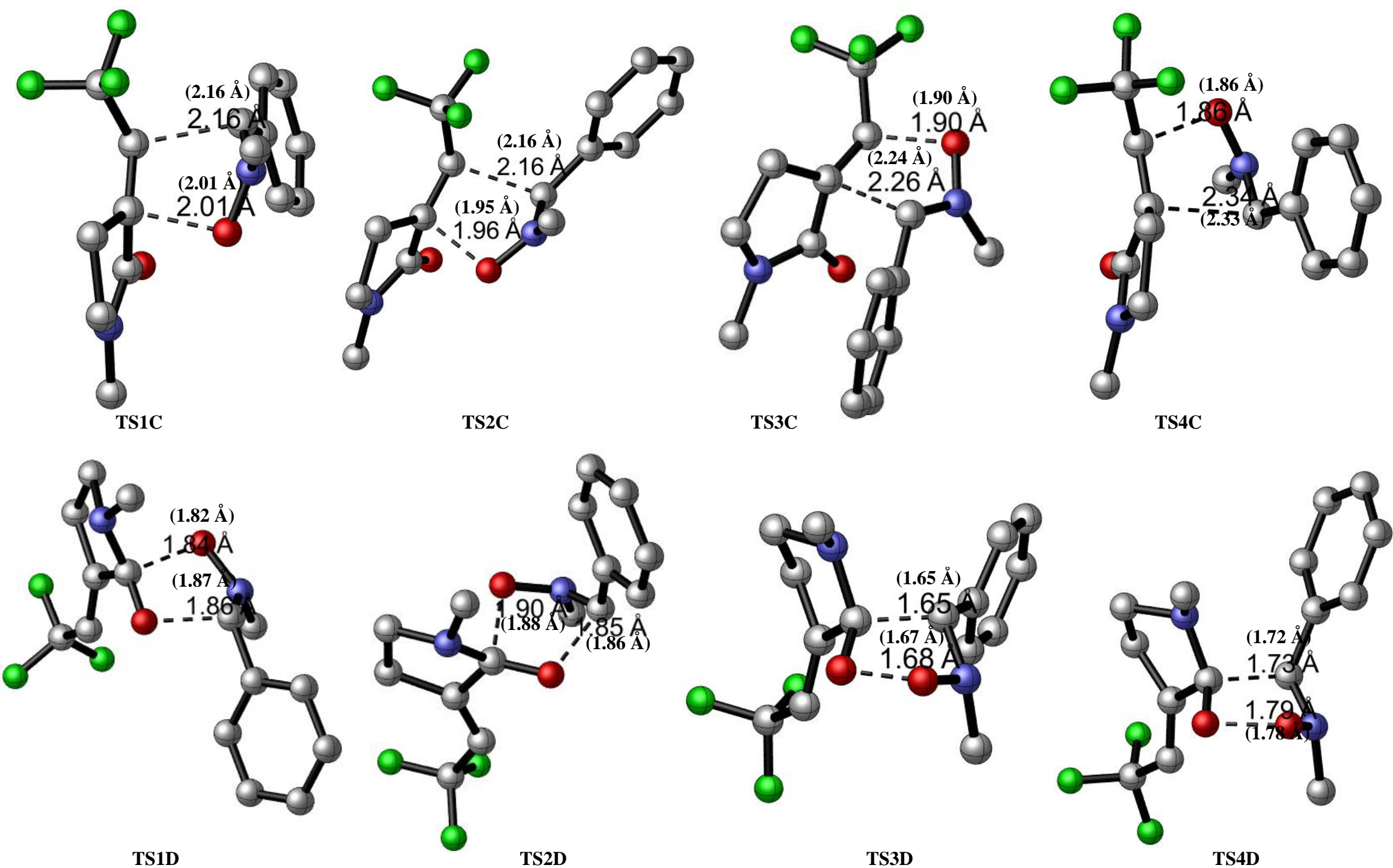
Figure 7: Optimized transition state structures involved in the eight chemo-, regio-, and diastereoisomeric reaction paths considered for the 32CA reaction of **A1** (R$_1$ = H) and **A3** (R$_3$ = Ph) at the M06-2X/6-311G(d,p) level of theory in the gas-phase. All labeled bond distances are in Angstrom (Å). Distances in toluene solvation are given in parentheses. All hydrogens have been omitted to ensure the simplicity of structures

Table 7: Rate constants (in s^{-1}) at 25°C for the 32CA reaction of **A1** (R_1 = H) and **A3** (R_3 = Ph) for the formation of the various products computed at the M06-2X/6-311G(d,p) level of theory in the gas phase.

Product	Rate constants (k[T])
P1C	1.3×10^8
P2C	1.1×10^8
P3C	1.3×10^{11}
P4C	1.3×10^9
P1D	1.4×10^{-1}
P2D	6.2×10^{-2}
P3D	9.1×10^{-29}
P4D	4.4×10^{-30}

3.2.3 Analysis of the Origin of the Chemoselectivity observed in the 32CA Reaction of 1-methyl-3-(2,2,2-trifluoroethylidene)pyrrolidin-2-one with *N*-methyl-*C*-phenyl nitrone with Local Reactivity Indices

Figure 8 shows the atomic labels of 1-methyl-3-(2,2,2-trifluoroethylidene)pyrrolidin-2-one (**A1**, R_1 = H, OH). In this segment, we employ the local electrophilic (P_K^+) and nucleophilic (P_K^-) Parr functions to examine the origin of the chemoselectivity observed in the 32CA of **A1** (R_1 = H, OH) with **A3** (R_3 = Ph). Both the Mulliken and NBO atomic spin densities (ASD) analyses have been employed.

Within the **A1** (R_1 = H, OH), atomic centers with the largest electron density are the preferred point of attachment by the **A3** (R_3 = Ph) molecule. From the table 8, pertaining to the electrophilic Mulliken spin densities, analysis of the reaction centers in the **A1** (R_1 = H, OH) shows that, C_2 = 0.427, C_3 = 0.201, C_4 = 0.117, O_1 = 0.149, C_6 = 0.509, C_7 = -0.017, C_8 = 0.184 and O_2 = 0.129. The relatively large electron density at C_2 and C_3 compared to C_4 and O_1 accounts for the chemoselective addition of the **A3** (R_3 = Ph) across the olefinic moiety of **A1** (R_1 = H). Likewise,

the larger electron density at C_6 and C_7 than C_8 and O_2 accounts for the preferential addition of **A3** (R_3 = Ph) across the olefinic bond of **A1** (R_1 = OH). A similar pattern is observed for the analysis of the reaction centers in the **A1** (R_1 = H, OH) with the NBO atomic spin density.
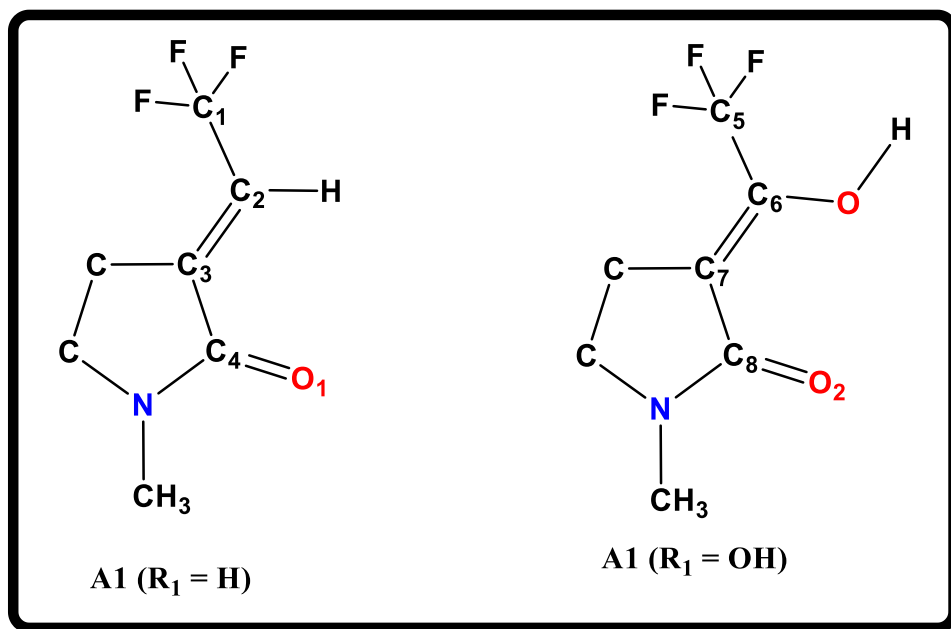
Figure 8: Atomic labels of 1-methyl-3-(2,2,2-trifluoroethylidene)pyrrolidin-2-one (**A1**, R_1 = H) .

Table 8: Mulliken and NBO atomic spin densities of 1-methyl-3-(2,2,2-trifluoroethylidene)pyrrolidin-2-one (**A1**, R_1 = H, OH)

	A1 (R_1 = H, OH)			**A1** (R_1 = H, OH)	
	NBO			MULLIKEN	
	ANION	CATION		ANION	CATION
C_1	-0.001	0.044	C_1	-0.003	0.049
C_2	0.027	0.395	C_2	0.033	0.427
C_3	-0.0	0.199	C_3	-0.002	0.201
C_4	0.004	-0.012	C_4	0.01	-0.030
C_5	-0.003	0.046	C_5	-0.006	0.054
C_6	0.083	0.471	C_6	0.095	0.509
C_7	0.041	0.014	C_7	0.039	-0.017
C_8	-0.061	0.157	C_8	-0.069	0.184
O_1	0.140	0.154	O_1	0.144	0.149
O_2	0.018	0.133	O_2	0.021	0.129

3.2.4 Effect of Substituents on the 32CA Reaction of (E)-1-methyl-3-(2,2,2-trifluoroethylidene)pyrrolidin-2-one with *N*-methyl-*C*-phenyl nitrone

In this segment, the 32CA reactions of EDGs- and EWGs-substituted nitrone with (E)-1-methyl-3-(2,2,2-trifluoroethylidene)pyrrolidin-2-one have been explored at the M06-2X/6-311G(d,p) level of theory in the gas phase and the results are shown in table 9.

The followingconclusions can be drawn from the energetics displayed in table 9: (a) similar to the reaction of **A1** (R_1 = H) and **A3** (R_3 = Ph), the reaction of EDGs- and EWGs-substituted nitrone **A3** (R_3 = EDGs, EWGs) with **A1** (R_1 = H) is highly chemoselective towards the exocyclic olefinic bond of **A1** (R_1 = H) (b) similar to the preferred pathway established in section 3.2.2 for the 32CA reaction of **A1** (R_1 = H) and **A3** (R_3 = Ph), the formation of **P3C** through **TS3C** is the most preferred pathway for all reactions studied except the reaction of **A1** (R_1 = H) and **A3** (R_3 = carbonyl) which proceeds through **TS4C** to **P4C** (c) in contrast to the reactions of **A1** (R_1 = H) and **A2** (R_2 = EDGs, EWGs), the electronic and steric nature of the substituents have little effect on the selectivities observed in the reaction of **A1** (R_1 = H) and **A3** (R_3 = Ph) (d) addition of the **A3** (R_3 = EDGs, EWGs) across the olefinic moiety of **A1** (R_1 = H) is highly exothermic whereas addition across the carbonyl moiety presents an endothermic reaction in most cases (e) the predominatant factor controlling the selectivites observed in the reactions of **A1** (R_1 = H) with nitrone derivatives is the kinetics of the reactions

Table 9: Activation and reaction energies of transition states and products respectively for the 32CA reaction of nitrone derivatives and **A1** (R_1 = H) at the M06-2X/6-311G(d,p) level of theory in the gas phase. All energies are in kcal/mol.

SUBSTITUENT (S) (R_3 = S)	TS1C	TS2C	TS3C	TS4C	TS1D	TS2D	TS3D	TS4D	P1C	P2C	P3C	P4C	P1D	P2D	P3D	P4D
Methyl	3.5	3.1	3.0	6.4	15.2	18.8	51.7	55.1	-34.3	-28.0	-30.3	-29.3	-2.3	-1.5	57.9	52.9
Ethyl	2.4	2.8	2.1	5.1	14.8	17.7	51.0	53.0	-32.8	-30.4	-26.5	-30.8	-3.3	-3.0	52.1	51.7
Amine	1.7	2.8	1.3	3.7	11.1	15.0	53.7	54.5	-30.9	-21.8	-28.2	-28.4	-0.8	0.4	59.6	-4.7
Thiol	8.1	4.7	2.9	7.9	16.2	21.4	51.1	-	-33.9	-27.7	-31.4	-29.9	-0.1	-0.6	56.2	52.4
Bromo	6.5	2.4	1.1	5.9	14.7	18.9	48.8	52.4	-37.7	-40.2	-34.8	-35.5	-4.5	-7.4		51.2
Chloro	5.2	1.5	0.2	5.2	13.4	17.2	47.6	51.0	-38.7	-40.7	-35.9	-36.4	-5.8	-8.7	52.3	50.1
Cyano	8.0	4.3	1.9	5.6	20.2	21.3	52.3	55.5	-32.8	-29.9	-31.5	-30.4	2.3	1.3	57.5	53.4
Carbonyl	3.9	7.5	3.7	2.8	23.0	20.1	56.7	53.7	-32.3	-24.8	-27.2	-30.6	3.8	2.7	52.6	54.9
Phenyl	6.4	6.5	2.3	5.0	18.6	19.1	55.7	57.5	-33.9	-22.0	-27.7	-28.5	0.1	0.3	52.6	52.1

3.2.5 Global Reactivity Indices Analysis of the 32CA Reaction of (E)-1-methyl-3-(2,2,2-trifluoroethylidene)pyrrolidin-2-one with Diazomethane Derivatives

The various global parameters (electronic chemical potential (μ), chemical hardness (η), global electrophilicity (ω), maximum electronic charge transfer (ΔN_{max}) and nucleophilicity values (N)) of the different nitrone derivatives have been computed to delineate the 32CA reaction between **A1** (R_1 = H, OH) and **A3**. The results of the analysis are shown in table 10. The μ value for **A1** (R_1 = H) is -4.55 eV, **A1** (R_1 = OH) is -4.11 eV and that of **A3** (R_3 = Ph) is -3.80 eV hence a FEDF reaction is expected in the 32CA reaction of **A1** (R_1 = H, OH) with **A3** (R_3 = Ph). This observation is consistent with the calculated GEDT values of the four competitive 32CA reaction pathways discussed in sections 3.2.1 and 3.2.2.

From table 10, EDGs-substituted nitrone molecules (**A3,** R_3 = methyl, ethyl, amine, thiol) have higher electronic chemical potential values relative to **A3** (R_3 = Ph). EDGs-substituted nitrone derivatives are strong electron-donating molecules hence a more polar reaction is expected in their 32CA reaction of **A1** (R_1 = H). Likewise, weak deactivating groups on the nitrone (**A3,** R_3 = bromo, chloro) also increase the chemical potential values relative to **A3** (R_3 = Ph). On the other hand, powerful deactivating groups on the nitrone molecule decrease the μ value regarding the **A3** (R_3 = Ph) molecule. The order of the electronic chemical potential for the various nitrone derivatives **A3** is given in the order carbonyl < cyano <phenyl < chloro < bromo < ethyl < thiol = methyl < amine.

The global electrophilicity (ω) [40] and maximum electronic charge transfer (ΔN_{max}) [52] are convenient tools used in the analysis of the reactivity of species participating in polar organic reactions. The electrophilicity index measures the stabilization energy when the system acquires an additional electronic charge ΔN_{max} from the environment, in terms of the electronic chemical potential μ and the chemical hardness η. A good electrophile is characterized by a high ω value

and low ΔN_{max} value. The nitrone molecule (**A3**, R_3 = Ph) is a moderate electrophile with a ω value of 1.1 eV. Evident from table 10, EDGs and weakly deactivating groups on the nitrone molecule significantly reduce the ω values whereas strongly deactivating groups increase the ω values. A similar trend is observed for the analysis of the calculated ΔN_{max} values for the nitrone derivatives.

With regards to the nucleophilicity values (N) [44] provided in table 10, **A3** (R_3 = cyano) has an N value of 0.91 eV, making it the poorest nucleophile in the nitrone series. Relative to EWGs-substituted nitrone, EDGs-nitrone derivatives have fairly higher N values. **A3** (R_3 = amine) with N value of 2.83 eV represents the best nucleophile.

Table 10: Global reactivity indices for the various nitrone derivatives (**A3**). Orbital energies are in eV.

SUBSTRATE (A3) R$_3$	HOMO	LUMO	μ	η	ω	ΔN_{max}	N
Methyl	-7.35	0.75	-3.30	8.10	0.67	0.41	2.01
Ethyl	-7.34	0.72	-3.31	8.06	0.68	0.41	2.03
Amine	-6.54	1.38	-2.58	7.91	0.42	0.33	2.83
Thiol	-7.12	0.52	-3.30	7.63	0.71	0.43	2.25
Bromo	-7.67	0.17	-3.75	7.84	0.90	0.48	1.69
Chloro	-7.74	0.21	-3.76	7.95	0.89	0.47	1.63
Cyano	-8.45	-1.13	-4.79	7.32	1.57	0.65	0.91
Carbonyl	-8.37	1.29	-4.83	7.08	1.65	0.68	0.99
Phenyl	-7.08	-0.51	-3.80	6.56	1.10	0.58	2.29
A1 (R_1 = H)	-8.56	-0.54	-4.55	8.01	1.29	0.57	0.81
A1 (R1 = OH)	-8.04	-0.17	-4.11	7.87	1.07	0.52	1.32

4.0   Conclusion

The reactions of diazomethane (**A2**) and *N*-methyl-*C*-phenyl nitrone (**A3**) derivatives with 1-methyl-3-(2,2,2-trifluoroethylidene)pyrrolidin-2-one derivatives (**A1**) occurs chemoselectively along the olefinic bond of **A1** via an asynchronous one-step mechanism. Analysis of the electrophilic (P_K^+) and nucleophilic (P_K^-) Parr functions at the different reaction sites in **A1** shows that the TACs (**A2**, **A3**) add across the atomic centers with the largest Mulliken and NBO atomic spin densities. The reactions of **A1** with **A2** and **A3** proceed via forward electron density flux (FEDF), where electron density fluxes from the three-atom components (**A2** and **A3**) to **A1**. The GEDT analysis has established an inverse relationship between the polar character of the reactions and activation barriers, the reactions with the highest polar character having the lowest barriers.

The calculated activation bariers and rate constants indicate substantial selectivity between the various diastereomers, with the formation of **P1A**, **P3A**, and **P1B** being highly favored over **P2A**, **P4A**, and **P2B** respectively. Negligible variation in both activation and reaction energies is observed for solvent phase (diethyl ether) computation for the 32CA reaction of **A1** ($R_1 = H$) with **A2** ($R_2 = H$). The energetic trends observed remain the same as in the gas phase computation. From the calculated chemical potential values of the diazomethanes derivatives, a more polar reaction is expected in the 32CA reaction of **A1** ($R_1 = H$) with **A2** ($R_2 = EDGs$) molecules than in the 32CA reaction of **A1** ($R_1 = H$) with **A2** ($R_2 = EDGs$) in which a less polar character.

The exergonic reaction that proceeds through **TS3C** to furnish **P3C** spirocycloadduct is the most kinetically favored pathway in all reaction routes considered for the 32CA reaction of **A1** ($R_1 = H$, OH) and **A3** ($R_3 = Ph$). The electronic and steric nature of substituents on the nitrone molecule does not influence the preferred pathway observed in the reaction of **A1** ($R_1 = H$) with **A3**

molecules. Toluene solvation has no susbstantial mechanistic effect on the 32CA reaction of **A1** (R$_1$ = H, OH) with *N*-methyl-*C*-phenyl nitrone.

Competing Interest

The authors declare that there is no conflict of interest whatsoever regarding the publication of this manuscript.

Supporting Information

The Supporting Information file contains Cartesian coordinates of all optimized geometries, harmonic vibrational frequencies, and the absolute energies of all products and transition states computed in this study.

ORCID
George Baffour Pipim: https://orcid.org/0000-0002-4700-8005

Richard Tia: https://orcid.org/0000-0003-1043-8869

Evans Adei: https://orcid.org/0000-0003-2544-8883

References

[1]   Domingo, L.R.; Ghodsi, F.; Ríos-Gutiérrez, M. *Molecules*, **2019** 24(22),4159.

[2]   Sannigrahi M.; *Tetrahedron*, **1999,** 55, 9007–9071.

[3]   Grygorenko, O.O.; Radchenko, D.S.; Volochnyuk, D.M.; Tolmachev, A.A.; Komarov, I.V. *Chem.l Rev.*, **201**1, *111*(9), 5506-5568.

[4]   Opoku, E.; Arhin, G.; Pipim, G.B.; Adams, A.H.,; Tia, R.; Adei, E.; *Theor.l Chem. Acc.*, **2020,** *139*(1), 1-15.

[5]   Zheng, Y.J.; Tice, C.M. *Expert opin Drug Discov*, **2016,** *11*, 831-834.

[6]   Chupakhin, E.; Babich, O.; Prosekov, A.; Asyakina, L.; Krasavin, M. *Molecules*, **2019,** *24*(22), 4165.

[7]   Carreira, E.M.; Fessard, T.C. *Chem. Rev.*,**2014,** 114, 8257–8322.

[8]   Kotha, S.; Panguluri, N.R.; Ali, R. *European J. Org. Chem.* **2017,** 2017, 5316–5342.

[9]   King, T.A.; Stewart, H.L.; Mortensen, K.T.; North, A.J.; Sore, H.F.; Spring, D.R. *European J. Org. Chem.* **2019,** 2019, 5219–5229.

[10]   Zheng, Y.; Tice, C.M.; Singh, S.B. *Bioorganic Med. Chem. Lett.* **2014,** 24, 3673–3682.

[11]   Marson, C.M. *Chem. Soc. Rev*. **2011,** 40, 5514–5533.

[12]   Müller, G.; Berkenbosch, T.; Benningshof, J.C.; Stumpfe, D.; Bajorath, *J. Chem. - A Eur. J.* **2017,** 23, 703–710.

[13]   Mokhtari, T.S.; Seifi, M.; Saheb, V.; Sheibani, H.; *Arab. J. Chem.* **2019,** 12 (2019) 2937–2942.

[14]   Klier, L.; Tur, F.; Poulsen, P.H.; Jørgensen, K.A. *Chem. Soc. Rev*. **2017,** 46, 1080–1102.

[15]   Pipim, G.B.; Opoku, E.; Tia, R.; Adei, E. J. *Mol. Graph. Model.* **2020,** 97, 107542-107553.

[16]   Pipim, G.B.; Tia, R.; Adei, E. *Mol. Graph. Model.* **2020,** 100, 107672-107683.

[17]   Ríos- Gutiérrez, M.; Domingo, L.R. *European J. Org. Chem*. **2019,** 2019, 267–282.

[18]   Nacereddine, A.K.; Sobhi, C., Djerourou A.; Ríos-Gutiérrez, M.; Domingo, L.R. *RSC Adv.* **2015,** 5, 99299–99311.

[19]   Pipim, G.B.; Tia, R.; Adei, E. *J. Phys. Org. Chem.* **2020,** 1–15.

[20]   Pipim, G.B.; Opoku, E., *J. Mol. Model.* **2021,** 27, 1–15.

[21]   Padwa, A.; Goldstein, S.I. *Can. J. Chem.* **1984,** 62, 2506–2514.

[22]   Cheng, B.; Bao, B.; Zu, B.; Duan, X.; Duan, S.; Li, Y.; Zhai, H. *RSC Adv.* **2017,** 7, 54087–54090.

[23]   Jegham, N.; Bahi, A.; El Guesmi, N.; Kacem, Y.; Hassine, B.B. *Arab. J. Chem.* **2017,** 10, 3889–3894.

[24]   Cacciarini, M.; Cordero, F.M.; Faggi, C.; Goti, A. *Molecules.* **2000,** 5, 637–647.

[25]   Bouillon, J.P.; Janousek, Z.; Viehe, H.G.; Tinant, B.; Declercq, J.P. *J. Chem. Soc. Perkin*

Trans. I **1996,** 15, 1853–1858.

[26]   Frisch, M. J.; Trucks, G. W.; Schlegel, H. B.; Scuseria, G. E.; Robb, M. A.; Cheeseman, J. R.; Scalmani, G.; Barone, V.; Mennucci, B.; Petersson G. A. et al. *Gaussian 09,* revision b, 01, Gaussian, Inc., Wallingford CT, **2009**.

[27]   Wavefunction, spartan 14' v.1.1.8, Wavefunction **2014.**

[28]   Zhao, Y.; Truhlar, D.G. *Acc. Chem. Res.* **2008**, 41, 157–167.

[29]   Pieniazek, S.N.; Houk, K.N. *Angew. Chemie - Int. Ed.* **2006,** 45, 1442–1445.

[30]   Paton, R.S.; Mackey, J.L.; Kim, W.H.; Lee, J.H.; Danishefsky, S.J.; Houk, K.N. *J. Am. Chem. Soc.* **2010,** 132, 9335–9340.

[31]   Paton, R.S.; Steinhardt, S.E.; Vanderwal, C.D.; Houk, K.N. *J. Am. Chem. Soc.* **2011,** 133, 3895–3905.

[32]   Wheeler, S.E.; Moran, A.; Pieniazek, S.N.; Houk, K.N. *J. Phys. Chem. A.* **2009,** 113, 10376–10384.

[33]   Opoku, E.; Tia, R.; Adei, E. *J. Phys. Org. Chem.* **2019,** 32, e3992.

[34]   Opoku, E.; Tia, R.; Adei, E. *J. Mol. Graph. Model.* **2019,** 92, 17–31.

[35]   Clark, M.; Cramer, R.D.; Van Opdenbosch. N. *J. Comput. Chem.* **1989,** 10, 982–1012.

[36]   Tomasi, J.; Mennucci, B.; Cammi, R. *Chem. Rev.* **2005,** 105, 2999–3093.

[37]   Opoku, E.; Tia, R.; Adei, E. *J. Chem.* **2016**, 10 pages.

[38]   Roland, D.; Haleegoah, J.N.; Opoku, E.; Tia, R.; Adei, E. *J. Mol. Graph. Model.* **2019,** 93 107452-107464.

[39]   C.Y. Legault, C. Y. CYLview. **2009.**

[40]   Domingo, L.R.; Aurell, M.J.; Pérez, P.; Contreras, R. *J. Phys. Chem. A.* **2002,** 106, 6871–6875.

[41]   Parr, R.G.; Szentpály, L.V.; Liu, S. *J. Am. Chem. Soc.* **1999,** 121, 1922–1924.

[42]   Koopmans, T. *Physica*. **1934,** 1,104–113.

[43]   Domingo, L.R.; Pérez, P.; Sáez, J.A. *RSC Adv.* **2013,** 3, 1486–1494.

[44]   Domingo, L.R.; Chamorro, E.; Pérez, P. *J. Org. Chem.* **2008,** 73, 4615–4624.

[45]   Domingo, L.R. *RSC Adv.* **2014,** 4, 32415–32428.

[46]   Reed, A.E.; Curtiss, L.A.; *Chem. Rev.* **1988,** 88, 899–926.

[47]   Reed, A.E.; Weinstock, R.B.; Weinhold, F. *J. Chem. Phys.* **1985,** 83, 735–746.

[48]   Ranck, J.P. *J. Chem. Educ.* **2001,** 78, 1024.

[49]   Domingo, L.R.; Ríos-Gutiérrez, M.; Pérez, P. *RSC Adv.* **2020,** 10, 15394–15405.

[50]   Domingo, L.R.; Kula, K.; Ríos-Gutiérrez, M. *J. Org. Chem.* **2020,** 2020, 5938–5948.

[51]   Mix, K.A.; Aronoff, M.R.; Raines, R.T. *ACS Chem. Biol.* **2016,** *11*, 3233-3244.

[52]   Domingo, L.R.; Ríos-Gutiérrez, M.; Pérez, P. *Molecules*. **2016,** 21, 748.